

Parkin and PINK1 mitigate STING-induced inflammation

Danielle A. Sliter¹, Jennifer Martinez², Ling Hao¹, Xi Chen³, Nuo Sun⁴, Tara D. Fischer¹, Jonathon L. Burman¹, Yan Li⁵, Zhe Zhang¹, Derek P. Narendra⁶, Huaibin Cai³, Max Borsche⁷, Christine Klein⁷ & Richard J. Youle^{1*}

Although serum from patients with Parkinson's disease contains elevated levels of numerous pro-inflammatory cytokines including IL-6, TNF, IL-1 β , and IFN γ , whether inflammation contributes to or is a consequence of neuronal loss remains unknown¹. Mutations in parkin, an E3 ubiquitin ligase, and PINK1, a ubiquitin kinase, cause early onset Parkinson's disease^{2,3}. Both PINK1 and parkin function within the same biochemical pathway and remove damaged mitochondria from cells in culture and in animal models via mitophagy, a selective form of autophagy⁴. The *in vivo* role of mitophagy, however, is unclear, partly because mice that lack either PINK1 or parkin have no substantial Parkinson's-disease-relevant phenotypes⁵⁻⁷. Mitochondrial stress can lead to the release of damage-associated molecular patterns (DAMPs) that can activate innate immunity⁸⁻¹², suggesting that mitophagy may mitigate inflammation. Here we report a strong inflammatory phenotype in both *Prkn*^{-/-} and *Pink1*^{-/-} mice following exhaustive exercise and in *Prkn*^{-/-}; *mutator* mice, which accumulate mutations in mitochondrial DNA (mtDNA)^{13,14}. Inflammation resulting from either exhaustive exercise or mtDNA mutation is completely rescued by concurrent loss of STING, a central regulator of the type I interferon response to cytosolic DNA^{15,16}. The loss of dopaminergic neurons from the substantia nigra pars compacta and the motor defect observed in aged *Prkn*^{-/-}; *mutator* mice are also rescued by loss of STING, suggesting that inflammation facilitates this phenotype. Humans with mono- and biallelic *PRKN* mutations also display elevated cytokines. These results support a role for PINK1- and parkin-mediated mitophagy in restraining innate immunity.

If mitophagy can function to remove damaged mitochondria to reduce the release of damage-associated molecular patterns (DAMPs), *Pink1*^{-/-} and *Prkn*^{-/-} mice would be expected to display increased levels of inflammatory cytokines. However, we found that cytokine levels in serum of *Prkn*^{-/-} and *Pink1*^{-/-} mice were similar to those in wild-type mice (Extended Data Fig. 1a). To acutely stress mitochondria, 12-week-old mice were exercised until exhausted for three consecutive days. No differences in the time to exhaustion were observed among wild-type, *Prkn*^{-/-} or *Pink1*^{-/-} mice (Extended Data Fig. 1b). Upon mitochondrial damage, PINK1 is stabilized on the outer mitochondrial membrane where it phosphorylates ubiquitin on Ser65, forming phospho-ubiquitin (pS65-Ub), which recruits and activates parkin, inducing mitophagy⁴. Therefore, to determine whether exhaustive exercise (EE) activates PINK1 *in vivo*, we quantified pS65-Ub levels in heart tissue. In wild-type heart, EE induced a twofold increase in pS65-Ub relative to control sedentary (SED) mice (Fig. 1a). In SED *Pink1*^{-/-} mice, pS65-Ub levels were lower than in wild-type SED mice and did not increase with EE (Fig. 1a). *Prkn*^{-/-} mice also did not display increased pS65-Ub following EE (Extended Data Fig. 1c). We directly measured mitophagy *in vivo* in heart tissue of wild-type and *Pink1*^{-/-} mt-Keima mice¹⁷. Consistent with pS65-Ub levels, mitophagy increased twofold

following EE in wild-type heart tissue relative to SED and was significantly lower following EE in *Pink1*^{-/-} mice relative to wild-type mice (Fig. 1b, c). Therefore, EE triggers PINK1 activation and mitophagy *in vivo*.

When mitophagy was increased in wild-type mice, there was no change in the serum concentration of IL-6, IFN β 1, IL-12(p70), IL-13, CXCL1, CCL2 or CCL4 either immediately or 24 hours after EE (Fig. 1d, e, Extended Data Fig. 1e-i). However, serum concentrations of these cytokines were markedly increased in serum of mitophagy-deficient *Prkn*^{-/-} and *Pink1*^{-/-} mice (Fig. 1d, e, Extended Data Fig. 1e-i). We found no differences in cytokines between SED wild-type and *Prkn*^{-/-} or *Pink1*^{-/-} mice, or between wild-type and *Lrrk2*^{G2019S/G2019S} mice following EE (Extended Data Fig. 1d, i). Moreover, after EE, *Pink1*^{+/-} mice had increased IL-6, IFN β 1, IL-12(p70), CXCL1 and CCL4, and *Prkn*^{+/-} mice displayed increased IL-6 (Extended Data Fig. 2a-f). We also examined serum from human *PRKN* and *PINK1* heterozygotes (Supplementary File 1). Consistent with previous reports, levels of IL-6, IL-1 β , CCL2, and CCL4 were higher in serum from patients with idiopathic Parkinson's disease than in serum from healthy controls (Fig. 2a, Extended Data Fig. 2g-i). Relative to control serum, levels of IL-6, IL-1 β , CCL2, and CCL4 in unaffected *PRKN* heterozygotes were significantly higher, and were comparable to levels in patients with idiopathic Parkinson's disease or patients with biallelic *PRKN* mutations, whereas the levels of these cytokines in serum of *PINK1* heterozygotes were similar to those in control serum (Fig. 2a, Extended Data Fig. 2g-i). Therefore, loss of Parkin also leads to an increase in inflammatory cytokines in humans before, or independent of, symptomatic neurodegeneration.

IL-6 is an endogenous pyrogen. As EE in *Prkn*^{-/-} and *Pink1*^{-/-} mice induced an increase of about 1000-fold in serum IL-6, we measured the body temperature of these mice. One day after EE, the surface body temperatures of *Prkn*^{-/-} and *Pink1*^{-/-} mice, but not those of wild-type mice, were significantly increased and remained elevated for 3 to 4 days before returning to baseline (Fig. 2b), consistent with the changes in serum cytokine levels (Fig. 2c, d, Extended Data Fig. 3d-i).

Mitochondrial dysfunction can trigger inflammation via the NLRP3 inflammasome and/or the cGAS-STING pathway⁸⁻¹². Although mitophagy can mitigate NLRP3-induced inflammation *in vitro*¹⁸, IL-1 β , a product of NLRP3 activation¹⁹, was not increased in *Prkn*^{-/-} or *Pink1*^{-/-} EE mice (Extended Data Fig. 1j), whereas the type I interferon IFN β 1, a product of STING activation^{15,16}, was increased (Fig. 1e). Therefore, we crossed *Prkn*^{-/-} and *Pink1*^{-/-} mice with STING *goldenticket* (*STING*^{gt/gt}; *Sting* is also known as *Tmem173*) mice²⁰ and subjected the crossed mice to EE. Time to exhaustion and baseline cytokine levels in *STING*^{gt/gt}, *Prkn*^{-/-}; *STING*^{gt/gt} and *Pink1*^{-/-}; *STING*^{gt/gt} mice were similar to those of wild-type mice (Extended Data Fig. 3a-c). In stark contrast to *Prkn*^{-/-} and *Pink1*^{-/-} mice following EE, *Prkn*^{-/-}; *STING*^{gt/gt} and *Pink1*^{-/-}; *STING*^{gt/gt} mice

¹Biochemistry Section, Surgical Neurology Branch, National Institute of Neurological Disorders and Stroke, National Institutes of Health, Bethesda, MD, USA. ²Immunity, Inflammation, and Disease Laboratory, National Institute of Environmental Health Sciences, National Institutes of Health, Research Triangle Park, NC, USA. ³Transgenics Section, Laboratory of Neurogenetics, National Institute of Aging, National Institutes of Health, Bethesda, MD, USA. ⁴Center for Molecular Medicine, National Heart, Lung and Blood Institute, National Institutes of Health, Bethesda, MD, USA. ⁵The Protein/Peptide Sequencing Facility, National Institute of Neurological Disorders and Stroke, National Institutes of Health, Bethesda, MD, USA. ⁶Neurogenetics Branch, National Institute of Neurological Disorders and Stroke, National Institutes of Health, Bethesda, MD, USA. ⁷Institute of Neurogenetics, University of Lübeck, Lübeck, Germany. *e-mail: youle@ninds.nih.gov

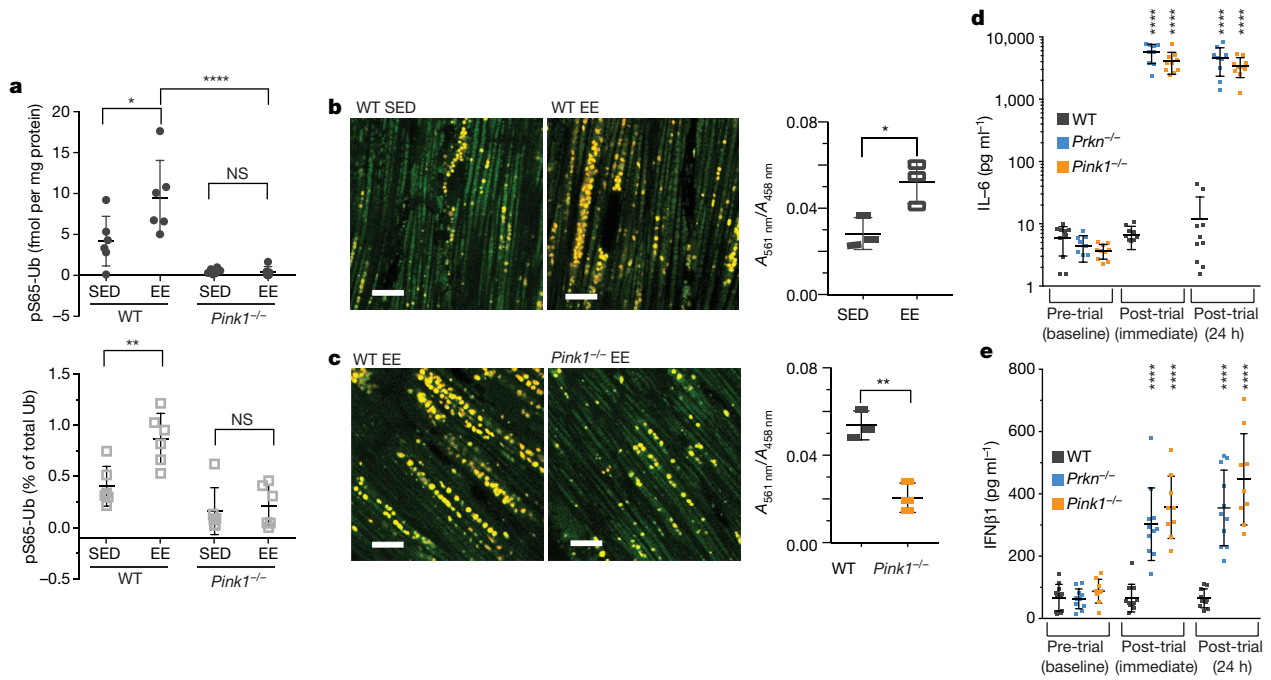


Fig. 1 | Inflammation and mitophagy in *Prkn*^{-/-} and *Pink1*^{-/-} mice. **a**, pS65-Ub in heart tissue, expressed as fmol per mg total protein (top), and as a percentage of total ubiquitin (bottom) (*n* = 6). WT, wild type. **b**, **c**, Left, representative images of heart tissue from SED or EE wild-type mice (**b**) or EE wild-type or *Pink1*^{-/-} mice (**c**) expressing mt-Keima; right,

*A*_{561 nm}/*A*_{488 nm} (*n* = 3). Scale bars, 10 μm. **d**, **e**, Serum IL-6 and IFNβ1 concentrations in EE mice (*n* = 10). Data are mean ± s.d.; individual data points are shown. **P* < 0.05, ***P* < 0.01, ****P* < 0.005, *****P* < 0.001, NS, not significant.

showed no detectable increase in the assayed cytokines (Fig. 2c, d; Extended Data Fig. 3d–i). Consistent with this finding, surface body temperature did not increase following EE in the absence of STING (Fig. 2b).

Since STING is activated when double-stranded DNA binds cyclic GMP-AMP synthase (cGAS), which in turn generates cyclic GMP-AMP (cGAMP)¹⁵, we examined serum DNA before and after EE. Both mtDNA copy number and the ratio of mitochondrial to nuclear DNA

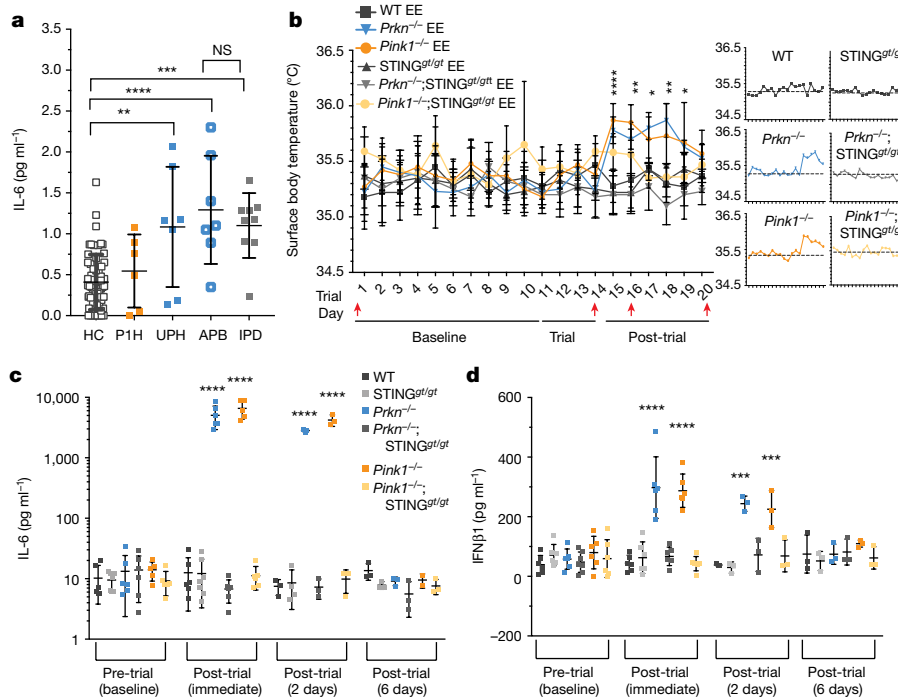


Fig. 2 | Inflammation in *Prkn*^{-/-} and *Pink1*^{-/-} mice following EE is completely rescued by loss of STING. **a**, Serum IL-6 concentration in humans: human control (HC) (*n* = 62), *PINK1* heterozygotes (PIH) (*n* = 6), unaffected *PRKN* heterozygotes (UPH) (*n* = 7), affected *PRKN* biallelic mutants (APB) (*n* = 7) and patients with idiopathic Parkinson's disease (IPD) (*n* = 9). **b**, Left, mean daily surface body temperature during

the trial. Red arrows indicate retro-orbital serum sampling. Right, average daily temperature relative to the average baseline temperature (grey dashed line) (*n* = 6). **c**, **d**, Serum IL-6 and IFNβ1 concentrations in EE mice before and after EE. *n* = 6, baseline and post-trial immediate; *n* = 3, post-trial, 2 days; *n* = 3, post-trial, 6 days). Data are mean ± s.d. Individual data points are shown (**a**, **c**, **d**).

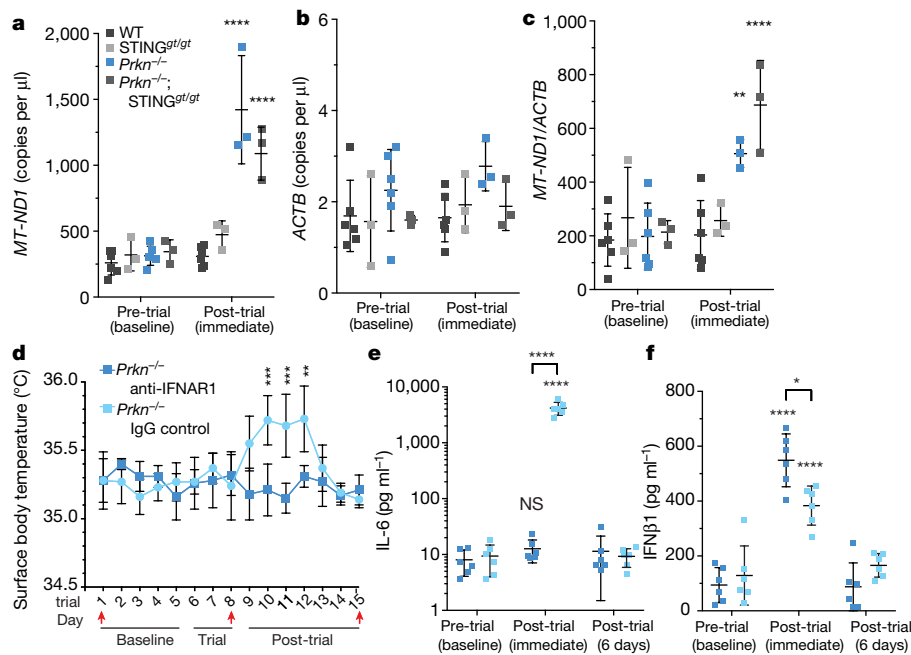


Fig. 3 | Increased circulating mtDNA in *Prkn*^{-/-} mice; IFNAR1-blocking antibody treatment blocks inflammation. a, b, Cell-free mtDNA (*MT-ND1*, a) and nuclear DNA (*ACTB*, b) in the serum of mice with the indicated genotype ($n \geq 3$). c, Ratio of mtDNA to nuclear DNA

in serum ($n \geq 3$). d, Mean daily surface body temperature during the trial ($n = 6$). Red arrows indicate retro-orbital sampling. e, f, Serum IL-6 and IFN β 1 concentrations in EE mice ($n = 6$). Data are mean \pm s.d. Individual data points are shown (a–c, e, f).

increased in the serum of *Prkn*^{-/-} and *Prkn*^{-/-};*STING*^{gt/gt} mice, but not in wild-type or *STING*^{gt/gt} mice, following EE (Fig. 3a–c). Additionally, liquid chromatography–mass spectrometry analysis revealed that 2',3'-cGAMP was markedly and comparably increased in heart tissue of *Pink1*^{-/-} and *Prkn*^{-/-} mice following EE, but was not detectable in wild-type or SED mice (Extended Data Fig. 4a). Treatment with a blocking antibody specific for interferon- α/β receptor subunit 1 (IFNAR1)²¹ inhibited the increase in body temperature and all serum cytokines except IFN β 1 (Fig. 3d–f, Extended Data Fig. 4c–g).

To determine whether EE-induced inflammation leads to tissue damage, we measured serum creatine kinase²². All genotypes had similar levels of serum creatine kinase at baseline, which increased following EE in *Prkn*^{-/-} and *Pink1*^{-/-} mice, but not in wild-type mice (Extended Data Fig. 5a). Notably, the increase in serum creatine kinase was not rescued by loss of STING or by pretreatment with IFNAR1-blocking antibody (Extended Data Fig. 5a, b), suggesting that mitophagy, as well as being important for mitigating inflammation, may also be critical for preventing muscle damage. This reveals another conditional phenotype in *Prkn*^{-/-} and *Pink1*^{-/-} mice, which is potentially related to the degeneration of flight muscles observed in parkin mutant *Drosophila*²³. Notably, parkin mutant *Drosophila* transcriptionally upregulate innate immune genes²⁴.

We also investigated inflammation in a chronic model of mitochondrial stress. Mice expressing a proofreading-defective mtDNA polymerase (*PolG*), called mutator, accumulate mutations in mtDNA, but do not exhibit neurodegeneration^{13,14}. However, *mutator* mice deficient in parkin exhibit dopaminergic neuron loss and a movement disorder that can be rescued by treatment with levodopa¹³. Serum cytokine levels were similar among 12, 20 and 40-week-old wild-type, *mutator* and *Prkn*^{-/-} mice (Fig. 4a, b, Extended Data Fig. 6a–h). However, *Prkn*^{-/-};*mutator* mice exhibited higher serum levels of IL-6, IFN β 1, TNF, IL-1 β , CCL2, IL-12(p70), IL-13, IL-17, CXCL1 and CCL4 at both 20 and 40 weeks of age, demonstrating considerable overlap with cytokines that are elevated in the EE-induced model of acute mitochondrial stress and human patients with Parkinson's disease (Fig. 4a–c, Extended Data Fig. 6a–h). Consistent with the EE model, loss of STING in *Prkn*^{-/-};*mutator* mice fully suppressed the inflammatory phenotype (Fig. 4a, b, Extended Data Fig. 6a–h). STING activation by binding of

cGAS to cytosolic double-stranded DNA (dsDNA), including mtDNA, and STING-mediated inflammation resulting from accumulation of mtDNA mutations in *mutator* mice indicate that mtDNA is the key inflammatory signal in the absence of parkin. Indeed, circulating mtDNA levels and ratios of mtDNA to nuclear DNA were higher in 40-week-old *Prkn*^{-/-};*mutator* mice compared to wild-type, *mutator* or *Prkn*^{-/-} mice, and loss of STING did not rescue the increase (Extended Data Fig. 7a–c). Unlike in the EE model, creatine kinase levels were not increased in aged *Prkn*^{-/-};*mutator* mice (Extended Data Fig. 5c).

To determine whether STING-mediated inflammation contributes to the motor defect previously reported in *Prkn*^{-/-};*mutator* mice¹³, we examined locomotor activity using a pole test that is sensitive to loss of dopaminergic neurons in mouse models of Parkinson's disease^{25,26}. There were no differences in the latency to descend among genotypes at 12 and 20 weeks of age (Fig. 4d, Extended Data Fig. 7d). However, 40-week-old *Prkn*^{-/-};*mutator* mice displayed a markedly increased latency to descend (Fig. 4d, Supplementary Video 1). The 40-week-old *Prkn*^{-/-};*mutator*;*STING*^{gt/gt} mice displayed latency times to descend that were indistinguishable from those of wild-type and *Prkn*^{-/-} mice (Fig. 4d, Supplementary Videos 2, 3). Furthermore, whereas 40-week-old *Prkn*^{-/-};*mutator* mice displayed a reduction of around 20% in neurons expressing tyrosine hydroxylase (TH⁺), concurrent loss of STING in the *Prkn*^{-/-};*mutator*;*STING*^{gt/gt} mice fully rescued TH⁺ neurons to wild-type levels (Fig. 4e, f). Even at 52 weeks of age, when *Prkn*^{-/-};*mutator* mice lose about 40% of TH⁺ cells¹³, *Prkn*^{-/-};*mutator*;*STING*^{gt/gt} mice displayed TH⁺ cell levels similar to those of wild-type mice (Extended Data Fig. 7e, f). Together, these data demonstrate a complete rescue of the motor defect and neurodegeneration in *Prkn*^{-/-};*mutator* mice in the absence of STING.

Parkin has been linked to adaptive immunity²⁷, and indeed, six weeks following EE, *Prkn*^{-/-} mice exhibited a marked increase in anti-nuclear antibodies (ANAs), whereas *Prkn*^{-/-} mice treated with IFNAR1 antibody or lacking STING activity did not (Extended Data Fig. 7g). Whereas antibodies against dsDNA were not detected in mice before or after EE, they (Extended Data Fig. 7h), but not ANAs, were significantly increased in both 20 and 40-week-old *Prkn*^{-/-};*mutator* mice but not in *Prkn*^{-/-};*mutator*;*STING*^{gt/gt} mice. Moreover, as in the chronic

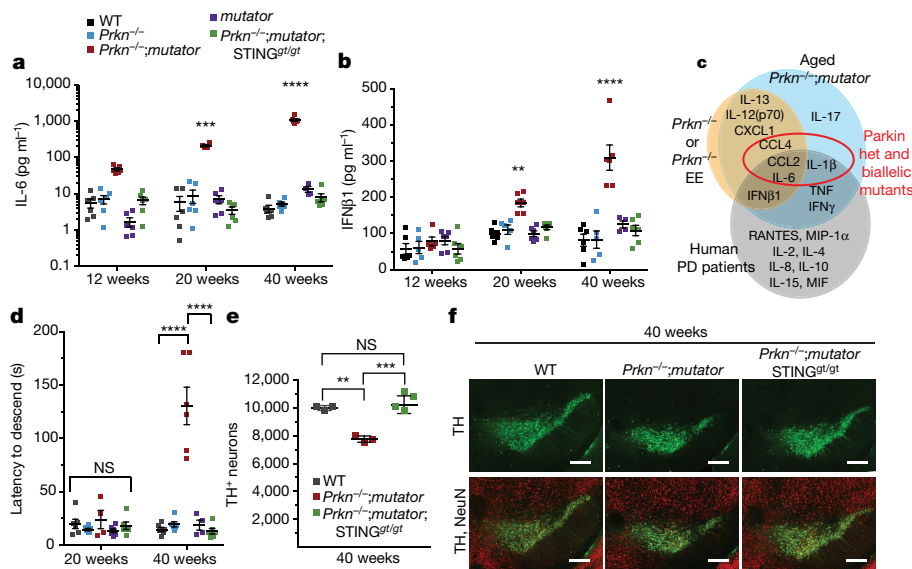


Fig. 4 | Loss of STING prevents inflammation, motor defect and neurodegeneration in the *Prkn*^{-/-};mutator mice. a, b, Serum IL-6 and IFN β 1 concentrations from 12, 20 and 40-week-old mice ($n = 4$ (IL-6), $n = 6$ (IFN β 1)). **c**, Venn diagram showing serum cytokines that were elevated in mouse models and in human patients with idiopathic Parkinson's disease (PD; grey)¹. **d**, Results of pole test ($n = 6$).

Prkn^{-/-};mutator stress model, the level of dsDNA antibodies, but not that of ANAs, was increased in the serum of patients with Parkinson's disease²⁸.

Here, we demonstrate that acute (EE-induced) and chronic (mtDNA mutation-induced) *in vivo* mitochondrial stress leads to a STING-mediated type I interferon response in mice in the absence of parkin or PINK1. Additionally, we found elevated cytokine levels in serum of asymptomatic human heterozygous *Prkn* mutation carriers. Intriguingly, intake of non-steroidal anti-inflammatory drugs is inversely associated with a later diagnosis of Parkinson's disease²⁹. Therefore, we hypothesize that parkin and PINK1 prevent inflammation and neurodegeneration by clearing damaged mitochondria, thereby preventing increases in cytosolic and circulating mtDNA, suggesting a new model for how mitophagy may mitigate Parkinson's disease. Supporting our findings, a recent report demonstrated that dopaminergic neurons in the substantia nigra have basal mitophagy rates higher than those of other dopamine-producing neurons³⁰.

Online content

Any methods, additional references, Nature Research reporting summaries, source data, statements of data availability and associated accession codes are available at <https://doi.org/10.1038/s41586-018-0448-9>

Received: 3 February 2018; Accepted: 23 July 2018;
Published online: 22 August 2018

- Dzambo, N., Geczy, C. L. & Halliday, G. M. Inflammation is genetically implicated in Parkinson's disease. *Neuroscience* **302**, 89–102 (2015).
- Kitada, T. et al. Mutations in the parkin gene cause autosomal recessive juvenile parkinsonism. *Nature* **392**, 605–608 (1998).
- Valente, E. M. et al. PINK1 mutations are associated with sporadic early-onset parkinsonism. *Ann. Neurol.* **56**, 336–341 (2004).
- Pickrell, A. M. & Youle, R. J. The roles of PINK1, parkin, and mitochondrial fidelity in Parkinson's Disease. *Neuron* **85**, 257–273 (2015).
- Goldberg, M. S. et al. Parkin-deficient mice exhibit nigrostriatal deficits but not loss of dopaminergic neurons. *J. Biol. Chem.* **278**, 43628–43635 (2003).
- Kitada, T. et al. Impaired dopamine release and synaptic plasticity in the striatum of PINK1-deficient mice. *Proc. Natl Acad. Sci. USA* **104**, 11441–11446 (2007).
- Perez, F. A. & Palmiter, R. D. Parkin-deficient mice are not a robust model of parkinsonism. *Proc. Natl Acad. Sci. USA* **102**, 2174–2179 (2005).

e, Neurons expressing tyrosine hydroxylase (TH⁺) counted by stereology in the substantia nigra of 40-week-old mice ($n = 3$ for wild type and *Prkn*^{-/-};mutator, and $n = 4$ for *Prkn*^{-/-};mutator;STING^{gt/gt}). **f**, Representative images of TH⁺ (green) and NeuN⁺ (total, red) neurons. Scale bars, 200 μ m. Data are mean \pm s.d.; individual data points are shown.

- Nakahira, K. et al. Autophagy proteins regulate innate immune responses by inhibiting the release of mitochondrial DNA mediated by the NALP3 inflammasome. *Nat. Immunol.* **12**, 222–230 (2011).
- Zhou, R., Yazdi, A. S., Menu, P. & Tschopp, J. A role for mitochondria in NLRP3 inflammasome activation. *Nature* **469**, 221–225 (2011).
- Rongvaux, A. et al. Apoptotic caspases prevent the induction of type I interferons by mitochondrial DNA. *Cell* **159**, 1563–1577 (2014).
- White, M. J. et al. Apoptotic caspases suppress mtDNA-induced STING-mediated Type I IFN production. *Cell* **159**, 1549–1562 (2014).
- West, A. P. et al. Mitochondrial DNA stress primes the antiviral innate immune response. *Nature* **520**, 553–557 (2015).
- Pickrell, A. M. et al. Endogenous Parkin preserves dopaminergic substantia nigral neurons following mitochondrial DNA mutagenic stress. *Neuron* **87**, 371–381 (2015).
- Trifunovic, A. et al. Premature ageing in mice expressing defective mitochondrial DNA polymerase. *Nature* **429**, 417–423 (2004).
- Chen, Q., Sun, L. & Chen, Z. J. Regulation and function of the cGAS–STING pathway of cytosolic DNA sensing. *Nat. Immunol.* **17**, 1142–1149 (2016).
- Ishikawa, H. & Barber, G. N. STING is an endoplasmic reticulum adaptor that facilitates innate immune signaling. *Nature* **455**, 674–678 (2008).
- Sun, N. et al. Measuring *in vivo* mitophagy. *Mol. Cell* **60**, 685–696 (2015).
- Zhong, Z. et al. NF- κ B restricts inflammasome activation via elimination of damaged mitochondria. *Cell* **164**, 896–910 (2016).
- Guo, H., Callaway, J. B. & Ting, J. P. Y. Inflammasomes: mechanism of action, role in disease, and therapeutics. *Nat. Med.* **21**, 677–687 (2015).
- Sauer, J.-D. et al. The *N*-ethyl-*N*-nitrosourea-induced *goldenticket* mouse mutant reveals an essential function of *Sting* in the *in vivo* interferon response to listeria monocytogenes and cyclic dinucleotides. *Infect. Immun.* **79**, 688–694 (2011).
- Sheehan, K. C. F. et al. Blocking monoclonal antibodies specific for mouse IFN- α/β receptor subunit 1 (IFNAR-1) from mice immunized by *in vivo* hydrodynamic transfection. *J. Interferon Cytokine Res.* **26**, 804–819 (2006).
- Brancaccio, P., Lippi, G. & Maffulli, N. Biochemical markers of muscular damage. *Clin. Chem. Lab. Med.* **48**, 757–767 (2010).
- Greene, J. C. et al. Mitochondrial pathology and apoptotic muscle degeneration in *Drosophila* parkin mutants. *Proc. Natl Acad. Sci. USA* **100**, 4078–4083 (2003).
- Greene, J. C., Whitworth, A. J., Andrews, L. A., Parker, T. J., and Pallanck, L. J. Genetic and genomic studies of *Drosophila* parkin mutants implicate oxidative stress and innate immune responses in pathogenesis. *Hum. Mol. Genet.* **14**, 799–811 (2005).
- Matsuura, K., Kabuto, H., Makino, H. & Ogawa, N. Pole test is a useful method for evaluating the mouse movement disorder caused by striatal dopamine depletion. *J. Neurosci. Methods* **73**, 45–48 (1997).
- Ogawa, N., Hirose, Y., Ohara, S., Ono, T. & Watanabe, Y. A simple quantitative bradykinesia test in MPTP-treated mice. *Res. Commun. Chem. Pathol. Pharmacol.* **50**, 534–541 (1985).
- Matheoud, D. et al. Parkinson's disease-related proteins PINK1 and Parkin repress mitochondrial antigen presentation. *Cell* **166**, 314–327 (2016).
- Benkler, M. et al. Immunology, autoimmunity, and autoantibodies in Parkinson's disease. *Clin. Rev. Allergy Immunol.* **42**, 164–171 (2012).

29. Noyce, A. J. et al. Meta-analysis of early nonmotor features and risk factors for Parkinson disease. *Ann. Neurol.* **72**, 893–901 (2012).
30. Guzman, J. N. et al. Systemic isradipine treatment diminishes calcium-dependent mitochondrial oxidant stress. *J. Clin. Invest.* **128**, 2266–2280 (2018).

Acknowledgements We thank the animal husbandry staff at NINDS and the staff of the Murine Phenotyping Core Facility at NHLBI; the Clinical Pathology Group in the Cellular & Molecular Pathology Branch at NIEHS for serum creatine kinase; K. Gerrish and B. Elgart from the NIEHS Molecular Genomics Core for serum mitochondrial and nuclear DNA isolation and quantification; J. Vargas and S. Humble for experimental assistance and T. Finkel, J. Kowalak, A. Oberst and M. Ward for helpful suggestions. This work was supported by the NINDS Intramural Research Program (R.J.Y.), NIH Intramural Research Program 1ZIAES10328601 (J.M.), the NIA Intramural Research Program (H.C.) the DFG FOR2488; P2 and a Pilot Grant from the Excellence Cluster Inflammation at Interfaces (C.K.), and by a career development award from the Hermann and Lilly Schilling Foundation (C.K.).

Reviewer information *Nature* thanks Z. Chen, I. Dikic and the other anonymous reviewer(s) for their contribution to the peer review of this work.

Author contributions The project was conceived by D.A.S., J.M. and R.J.Y. Mouse experiments including EE, sample collection and behavioural studies were conducted by D.A.S. Serum analysis was performed by J.M. Mass spectrometry was performed by L.H. and Y.L. Neuron counting was performed by X.C. and H.C. mt-Keima analysis was performed by N.S. LRRK2 mutant mice were exercised by T.D.F. J.L.B. and Z.Z. provided technical assistance. Human patient samples were provided by D.P.N., M.B. and C.K. Writing and editing by D.A.S., J.M., C.K. and R.J.Y. Funding was provided to J.M., H.C, D.P.N, C.K. and R.J.Y.

Competing interests The authors declare no competing interests.

Additional information

Extended data is available for this paper at <https://doi.org/10.1038/s41586-018-0448-9>.

Supplementary information is available for this paper at <https://doi.org/10.1038/s41586-018-0448-9>.

Reprints and permissions information is available at <http://www.nature.com/reprints>.

Correspondence and requests for materials should be addressed to R.J.Y.

Publisher's note: Springer Nature remains neutral with regard to jurisdictional claims in published maps and institutional affiliations.

METHODS

No statistical methods were used to predetermine sample size. The experiments were not randomized. The investigators were blinded to allocation during certain experiments and outcome assessment as specified in the methods.

Mouse strains. All mice were housed in pathogen-free facilities under 12-h light dark cycles with access to food and water ad libitum. The STING *golden-ticket* (STING^{gt/gt}) mouse was obtained from Jackson Laboratories (C57BL/6J-Tmem173gt/J). It was generated by a chemically-induced mutation causing a T to A transversion which resulted in a point mutation at L199¹⁹. The point mutation triggers protein degradation and consequently, STING^{gt/gt} mice do not express STING or produce type I interferons in response to cyclic di-nucleotides¹⁹. Wild-type (C57BL/6J), *Prkn*^{-/-} (B6.129S4-Park2^{tm1Shn/l}), *Pink1*^{-/-} (B6.129S4-Pink1^{tm1Shn/l}) and *mutator* (B6.129S7 (Cg)-Polg^{tm1Tpro/l}) mice were obtained from Jackson Laboratories. *Prkn*^{-/-} and *Pink1*^{-/-} mice were crossed with STING^{gt/gt} mice to generate *Prkn*^{-/-};STING^{gt/gt} or *Pink1*^{-/-};STING^{gt/gt} mice. *Prkn*^{-/-}; *mutator* mice were generated as described¹³ and crossed with *Prkn*^{-/-};STING^{gt/gt} mice to generate *Prkn*^{-/-}; *mutator*;STING^{gt/gt} mice. Owing to increased mtDNA mutational load and reduced fertility all *mutator* matings were performed with heterozygous mice. *Lrrk2*^{G2019S/G2019S} mice were obtained from Novartis by H. Cai (NHLBI) and generated as described³¹. mt-Keima mice on the FVB/NJ background were obtained from N. Sun, NHBLI and generated as described¹⁶. *Pink1*^{-/-} mice were crossed with mt-Keima mice to generate *Pink1*^{-/-} mice expressing mt-Keima. Genotypes were confirmed by PCR^{5,6,19,32}. All mice, except mt-Keima mice, have the nuclear background of C57BL/6J. All animal studies were carried out as approved by the Animal Care and Use Committee of the National Institute for Neurological Disorders and Stroke or the National Heart, Lung and Blood Institute.

Exhaustive exercise. To induce mitochondrial stress, we subjected mice to forced exhaustive treadmill running on a Columbus Eco 3/6 (Columbus Instruments). Ten-week-old mice were randomly assigned into sedentary (SED) and exhaustive exercise (EE) groups. All groups were counterbalanced by gender. At 11 weeks old, EE mice were familiarized with the treadmill using three days of low intensity running. On day 1 of the familiarization protocol, mice placed on the treadmill were given 5 min to acclimate before the treadmill belt was engaged. The belt speed was initially set to 8m/min then increased to 10m/min, then 12m/min for 5 min each, all at an incline of 10%. On day 2, mice were given 2 min to acclimate to the treadmill then exercised at 8m/min, 10m/min, 12m/min and 15m/min for 5 min each. On day 3, mice were placed on the treadmill and immediately exercised at 10m/min for 5 min, then 12m/min, 15m/min and 18m/min for 5 min each. After familiarization, mice were allowed two days to recover before beginning the EE protocol. For three consecutive days, mice were subjected to the following protocol: At a 10% incline, the initial speed was set at 10m/min for 8 min, then increased to 15m/min for 5 min, and then increased by 1.8m/minute every three minutes until reaching a speed of 22.4m/minute. Mice were exercised for 10 min at 22.4m/min, then speed was then increased by 1m/min every 5 min until exhaustion. Exhaustion was determined when the mice failed to re-engage all four paws with the treadmill belt despite negative stimulus. For each EE experiment, the number of mice were listed per experimental group in the figure legends and individual data points were graphed. The experimenter was blinded to the genotype of the mouse being exercised.

Blood collection and analysis. Blood was drawn from the retro-orbital sinus of SED and EE mice anesthetized with isoflourane using heparinized capillary tubes. Baseline blood draws were performed on 10-week-old mice before exercise. Post-trial immediate blood draws were collected within 10 min of completion on the third day of the EE protocol. Final blood draws were performed at 24 h, 2 days, 6 days or 6 weeks after completion of the EE protocol. The same mouse was sampled for each time point (baseline, post-trial immediate and post-trial final). Serum was analysed in a blinded manner for cytokines using Bio-plex Pro Mouse Cytokine Standard 23-Plex, Group 1 (Bio-Rad) and Legend MAX Mouse IFN- β ELISA kit (BioLegend) and Mouse Anti-Nuclear Antigens (ANA/ENA) Ig's (total (A+G+M)) ELISA Kit (Alpha Diagnostics). Creatine kinase (CK) was measured using a modified International Federation of Clinical Chemistry (IFCC) method³³. Briefly, CK reversibly catalyses the transfer of a phosphate group from creatine phosphate to ADP, resulting in creatine and ATP. ATP is used to produce glucose-6-phosphate and ADP from glucose. The glucose-6-phosphate is oxidized with simultaneous reduction of the coenzyme NADP to give NADPH and 6-phosphogluconate. Therefore, the activity of CK is measured as U/ml directly proportional to the formation of NADPH. Reactions were carried as previously described, and A_{340 nm}/A_{600 nm} was read on an Olympus AU400e clinical analyser (Beckman Coulter). Circulating cell-free mtDNA and nuclear DNA was isolated from serum using the Maxwell RSC ccfDNA Plasma Kit (Promega) using the Maxwell RSC Instrument (Promega), then quantified using digital droplet PCR on a Maxwell as described³⁴. The assay used to detect *MT-ND1* was dMmuCNS343824284 (Bio-rad), and the assay used to detect *ACTB* was dMmuCNS292036842 (Bio-Rad).

Pole test. The pole test was performed as previously described^{13,25} to test the motor coordination of mice beginning at 12 weeks old, and then repeated at 20 and 40 weeks old. Mice were placed facing upward at the top of a vertical pole and given 180 s to change orientation and descend the pole. Failure to descend or falling from the pole was assigned 180 s. Each mouse performed the trial three times and the average latency to descend was determined. One day following the pole test, the same mouse also had blood drawn for cytokine analysis via the retro-orbital sinus, resulting in three pole tests and three blood draws per mouse, at 12, 20 and 40 weeks of age.

Quantification of TH⁺ neurons by stereology. According to the mouse brain in stereotaxic coordinates, a series of coronal sections across the midbrain (40 μ m per section, every third section from bregma -2.54 mm to -4.16 mm) were chosen and processed for tyrosine hydroxylase (TH) (ImmunoStar, Cat# 22941) and NeuN (Abcam, Cat# ab104225) staining, and visualized using a laser scanning confocal microscope (LSM 880; Zeiss). We examined 11–13 sections per brain. The images were captured as a projected layer at 20 μ m (pinhole, 10 μ m; interval, 5 μ m, 3–4 layers) under 10 \times magnification. The number of TH⁺ neurons was assessed using the fractionator function of Stereo Investigator 11 (MicroBrightField). The sampling scheme was designed to have coefficient of error (CE) of less than or equal to 5% in order to get reliable results. To achieve suitable CE, normally 12 serial sections, with a total of 140 counting frames were assessed. The final parameters of these studies were as follows: grid size, 250 \times 250 μ m; frame size, 200 \times 200 μ m. Three or four mice were used per genotype. Counters were blinded to the genotypes of the samples.

Body temperature sampling. Surface body temperature measurements were performed on SED and EE mice using the Exergen Temporal Scanner (TAT-5000, Exergen) beginning the day after the 10-week baseline blood draw and continuing daily until mice were euthanized either 2 days or 6 days after the exhaustive running protocol was complete. On days when mice were run or bled, temperatures were collected before exercise or blood draws. Mice were restrained by hand and the scanner was drawn across the abdomen from the left shoulder to the right hip. An average of three consecutive scans were recorded and the mean was calculated. For each mouse, baseline surface temperature was determined by collecting temperature for 11 days beginning the day after the baseline blood draw until beginning of the exercise trial. The average baseline temperatures depicted in the small graph insets in Fig. 2b were determined by averaging all baseline surface temperatures for each individual mouse (11 days). Surface body temperature sampling was routinely performed between 2 and 3 pm.

Anti-IFNAR1/2 blocking antibody treatment. *Prkn*^{-/-} mice were randomly assigned to control and treatment groups. Treatment began following the familiarization protocol one day before starting EE via intraperitoneal injection with 2.5 mg purified functional grade anti-IFNAR1 antibody (MAR1-5E3, catalogue number I-403, Leinco Technologies) or 2.5 mg purified functional grade anti-human interferon gamma receptor alpha as an IgG control²⁰ (GIR 208, catalogue number I-443, Leinco Technologies). This dose of anti-IFNAR1 has a half life of 5 days²⁰. Mice received only one treatment. The experimenter was blinded to the drug treatment. Three mice were treated with IgG control or anti-IFNAR1 in two separate trials for a total of $n = 6$ animals.

Quantification of pS65 ubiquitin and cGAMP in heart tissue. Ubiquitin and pS65 ubiquitin measurements were conducted as described¹³ with several modifications. In brief, EE and SED mice were perfused with phosphate-buffered saline, hearts were dissected and snap frozen in liquid nitrogen. For protein extraction, heart tissue was homogenized in an ice-cold lysis buffer (50 mM Tris/HCl pH 7.5, 150 mM NaCl, 0.1% SDS, 1% Triton, 1 mM DTT, 50 μ M PR-169, 5 mM *o*-phenanthroline, protease inhibitor cocktail (Roche), and phosphatase inhibitor cocktail (Roche). For ubiquitin enrichment, 4 mg of total protein from each sample was incubated overnight with Tandem Ubiquitin Binding Entities (TUBE, LifeSensors), washed four times with lysis buffer and another four times with 50 mM ammonium bicarbonate, eluted with 6 M guanidine HCl, precipitated with TCA, spiked with 200 fmol of UB-AQUA reference peptides (JPT Peptide Technologies), digested with Trypsin/Lys-C mix (Promega), and purified by HLB solid phase extraction column (Oasis). Purified peptides were dried down and redissolved in 0.1% formic acid in 2% acetonitrile. Targeted peptide analysis was performed on an UltiMate 3000 nanoLC system coupled with a Q Exactive HF mass spectrometer (Thermo). A 60 min liquid chromatography gradient was established on an EASY-Spray C18 column (Thermo, 2 μ m, 100 \AA , 75 μ m \times 250 mm) with a flow rate of 0.3 μ l/min. Buffer A was 0.1% formic acid in 2% acetonitrile, and buffer B was 0.1% formic acid and 5% DMSO in 95% acetonitrile. Targeted MS/MS scans were acquired with an isolation window of 1.4 m/z , higher-energy collisional dissociation (HCD) with a normalized collision energy of 25%, a resolution of 15 K, an automatic gain control of 5 \times 10⁵, and a maximum injection time of 50 ms. Raw data were uploaded onto Skyline 3.7³⁵ for data analysis and the results were exported to an Excel spreadsheet for subsequent statistical analysis^{13,36}. To quantify cGAMP, cGAMP was extracted and enriched from mouse heart samples following the steps described³⁷. Targeted

LC–MS experiment was conducted on a Dionex Ultimate 3000 nano liquid chromatography system coupled with a Fusion Lumos Mass Spectrometer. cGAMP was separated with a 40 min gradient on an EASY-Spray C18 column (Thermo, 2 μ m, 100 Å , 75 μ m \times 250 mm) with a flow rate of 0.3 μ l/min. Buffer A was 0.1% formic acid in 2% acetonitrile, and buffer B was 0.1% formic acid and 5% DMSO in 95% acetonitrile. Target m/z was 675.1080 with an isolation window of 2 Da, a resolution of 7.5K, an automatic gain control of 2×10^5 , and a maximum injection time of 32 ms. Raw data were acquired and analysed in Xcalibur software.

Assessing cardiac mitophagy using the mt-Keima transgenic mice. Cardiac mitophagy was measured using confocal microscopy as previously described¹⁷. In brief, for the hearts, tissues were rapidly dissected out, rinsed with cold PBS, and then further processed into small pieces (approximately 100 mm³). These sections were placed onto a 35-mm coverglass #1.5 bottom micro-well dish (MatTek) and analysed immediately. Fluorescence of mt-Keima was imaged in two channels via two sequential excitations (458 nm, green; 561 nm, red) and using a 570 to 695-nm emission range with a Zeiss LSM 780 confocal microscope (Carl Zeiss MicroImaging) equipped with a Plan-Apochromat 20 \times /0.8 NA, 40 \times /1.4 NA, and 63 \times /1.40 NA oil immersion objective lens. Laser power was set at the lowest output that would allow clear visualization of the mt-Keima signal. Imaging settings were maintained with the same parameters for comparison between different experimental conditions. Representative confocal images were processed using Imaris software by contrast linear stretch only. The average of four images from each tissue sample was taken, and calculation of mitophagy based on mt-Keima signal was performed employing the original images using Zeiss ZEN software on a pixel-by-pixel basis as previously described³⁸.

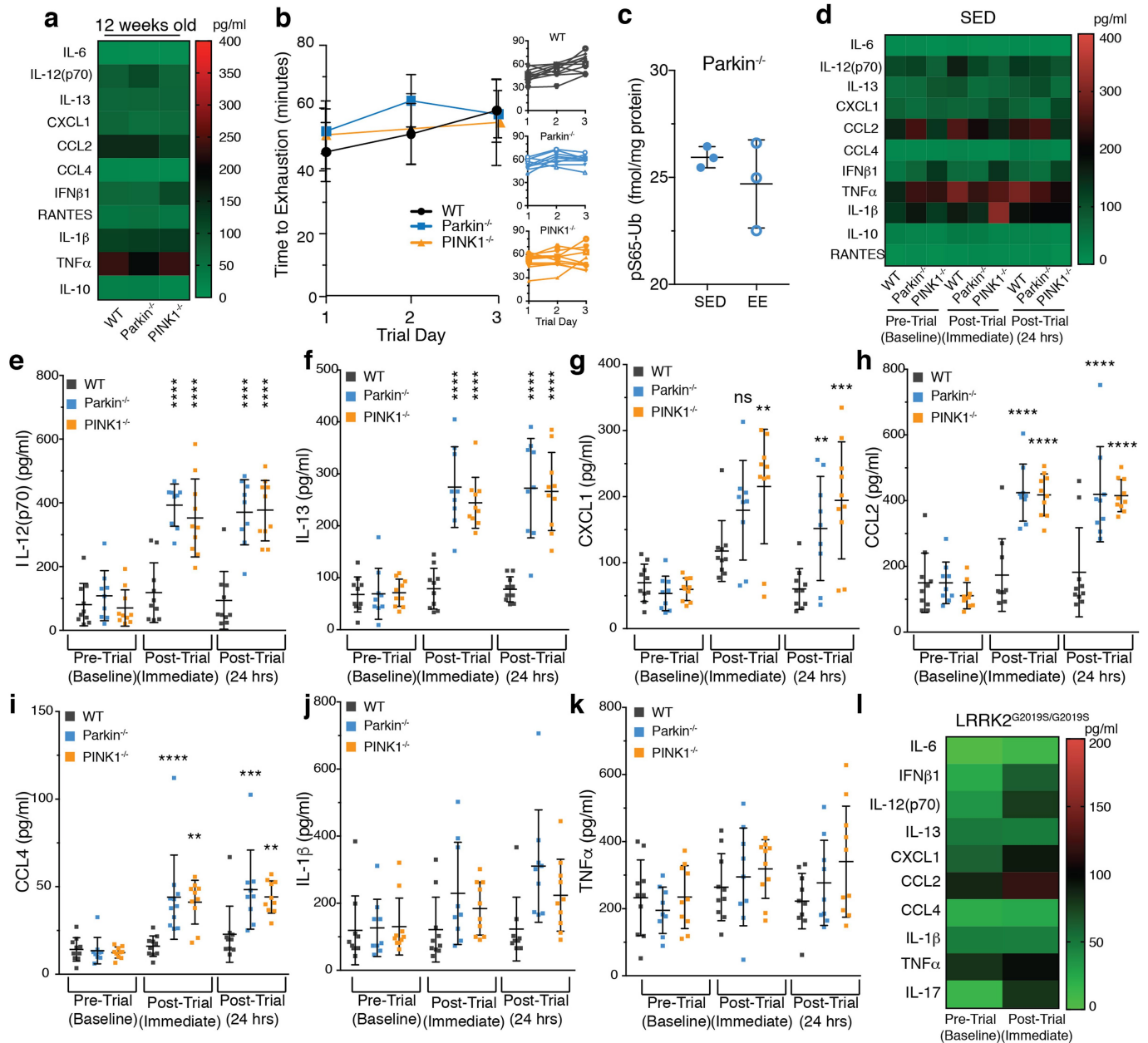
Recruitment and characterization of probands and serum sampling. All probands were recruited at the Institute of Neurogenetics and Department of Neurology of the University of Luebeck, a tertiary referral centre for movement disorders, or the National Institutes of Health (NIH) Clinical Center. Samples from the University of Luebeck were collected within the EPIPARK cohort³⁹, now part of the larger ProtectMove cohort which is enriched for patients with idiopathic Parkinson's disease recruited at the centre's outpatient clinics and containing a nested monogenic Parkinson's disease/asymptomatic mutation carrier cohort. The local IRB granted approval of the Parkinson's disease cohort and genetic studies. Samples from the NIH Clinical Center were collected under a protocol approved by the NIH Combined Neuroscience (CNS) Institutional Review Board. All patients and controls gave written informed consent and were neurologically examined by a movement disorder specialist. If applicable, a clinical diagnosis of Parkinson's disease was established according to the UK Brain Bank Criteria. Clinical characterization and ancillary tests included the UPDRS, Hoehn and Yahr, and MoCA score, as well as olfactory testing using the Brief Smell Identification Test. A blood

sample was obtained for extraction of DNA and preparation of serum. Genetic testing was performed with the Global Screening Array containing custom content for known Parkinson's disease genes and risk factors (Illumina), Sanger sequencing of Parkinson's disease-related genes, and multiplex ligation-dependent probe amplification (MLPA) to detect gene dosage changes. Serum was analysed in a blinded manner for cytokines using Bio-Plex Pro Human Cytokine 17-plex Assay (Biorad). **Statistical analysis.** Statistical analysis for multiple comparisons were performed in Prism 7 software using a two-way ANOVA on non-matched samples. All comparisons were to the same genotype, either before EE (pre-trial baseline) or to 12-week old animals shown in Fig. 4, unless otherwise noted with brackets. Human cytokines comparisons (Fig. 2a) were relative to controls unless noted by brackets. Body temperature comparisons were to the average temperature of wild-type mice measured on the same day.

Reporting summary. Further information on research design is available in the Nature Research Reporting Summary linked to this paper.

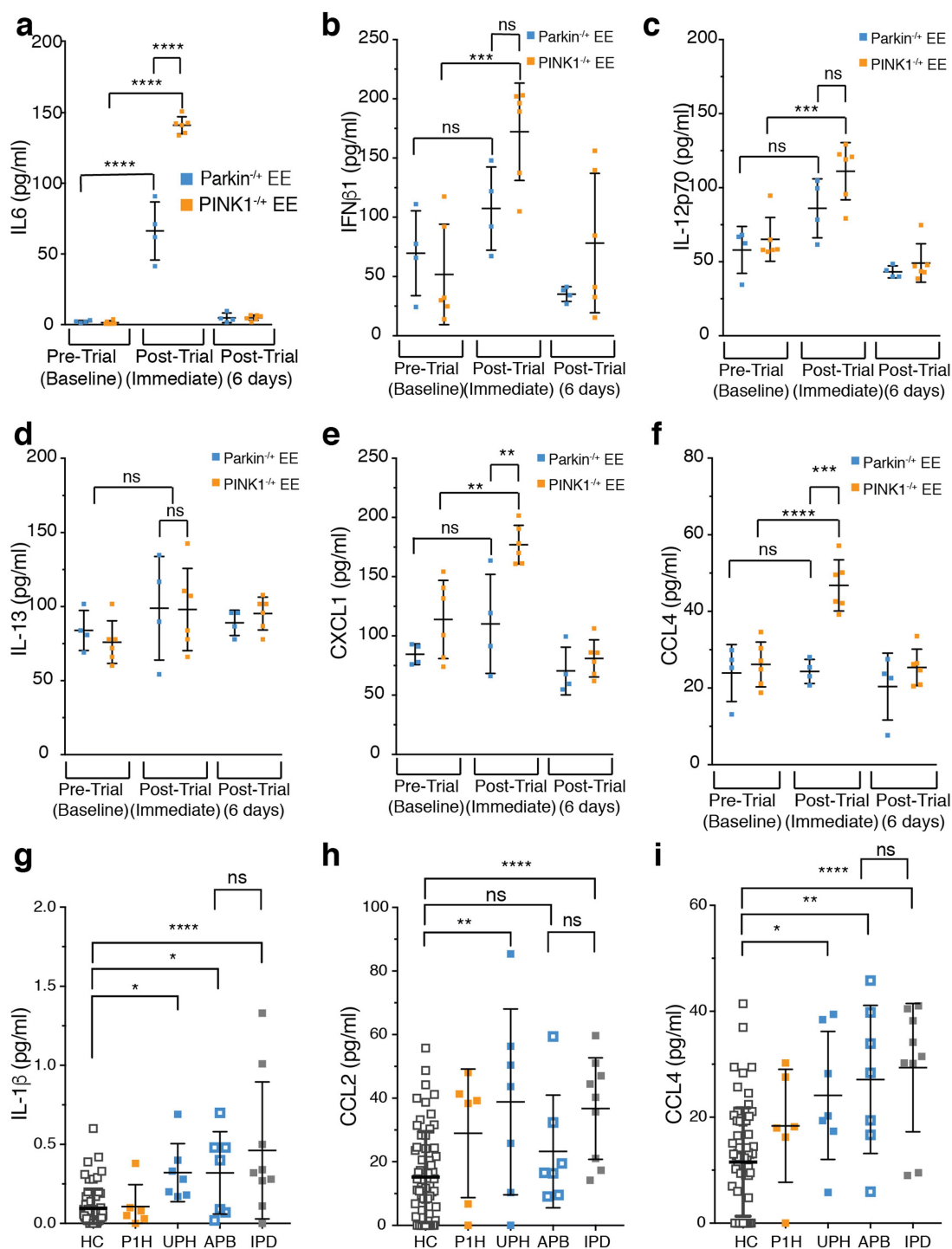
Data availability. LC-MS data that support the findings of this study are freely available to the public on Open Science Framework (https://osf.io/g5zfk/?view_only=2dc5b53dcf1747379ed1ea798eb705f5). All other relevant data are available in the manuscript.

- Herzig, M. C. et al. LRRK2 protein levels are determined by kinase function and are crucial for kidney and lung homeostasis in mice. *Hum. Mol. Genet.* **20**, 4209–4223 (2011).
- Kujoth, G. C. et al. Mitochondrial DNA mutations, oxidative stress and apoptosis in mammalian aging. *Science* **309**, 481–484 (2005).
- Horder, M. et al. International Federation of Clinical Chemistry, Scientific Division Committee on Enzymes: approved recommendation on IFCC methods for the measurement of catalytic concentration of enzymes. Part 7. IFCC method for creatine kinase (ATP: creatine *N*-phosphotransferase, EC 2.7.3.2). *Eur. J. Clin. Chem. Clin. Biochem.* **29**, 435–456 (1991).
- Ye, W. et al. Accurate quantitation of circulating cell-free mitochondrial DNA in plasma by droplet digital PCR. *Anal. Bioanal. Chem.* **409**, 2727–2735 (2017).
- MacLean, B. et al. Skyline: an open source document editor for creating and analyzing targeted proteomics experiments. *Bioinformatics* **26**, 966–968 (2010).
- Phu, L. et al. Improved quantitative mass spectrometry methods for characterizing complex ubiquitin signals. *Mol. Cell. Proteomics* **10**, M110.003756 (2011).
- Gao, D. et al. Activation of cyclic GMP-AMP synthase by self-DNA causes autoimmune diseases. *Proc. Natl Acad. Sci. USA* **112**, E5699–E5705 (2015).
- Sun, N. et al. A fluorescence-based imaging method to measure in vitro and in vivo mitophagy using mt-Keima. *Nat. Protoc.* **12**, 1576 (2017).
- Kasten, M. et al. Cohort profile: a population based cohort of study non-motor symptoms in parkinsonism (EPIPARK). *Int. J. Epidemiol.* **42**, 128–128 (2013).



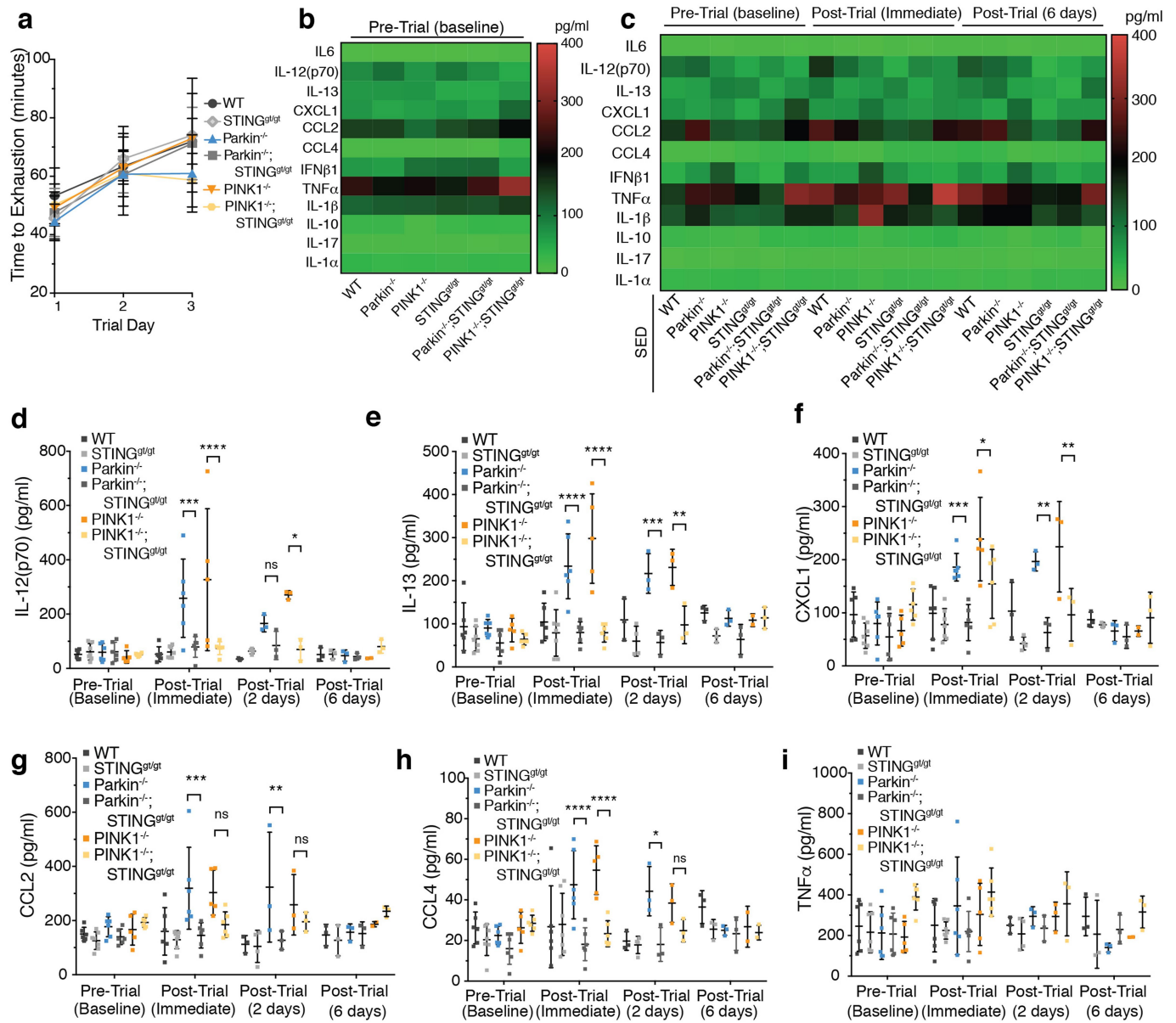
Extended Data Fig. 1 | Inflammation in *Prkn*^{-/-} and *Pink1*^{-/-} mice.
a, d, Heat maps depicting average cytokine concentration in serum from mice ($n = 10$). **b,** Average time to exhaustion on each trial day. Small graphs show individual run times ($n = 10$). **c,** pS65-ubiquitin in *Prkn*^{-/-} heart tissue expressed as fmol per mg total protein ($n = 3$). **e-k,** Serum

cytokine concentrations from EE mice are plotted as mean \pm s.d. ($n = 10$). **l,** Heat map depicting serum cytokine levels of *Lrrk2*^{G2019S/G2019S} ($n = 4$). Using t -tests, no differences in cytokine concentrations were found between pre-trial (baseline) and post-trial (immediate). ns, not significant.



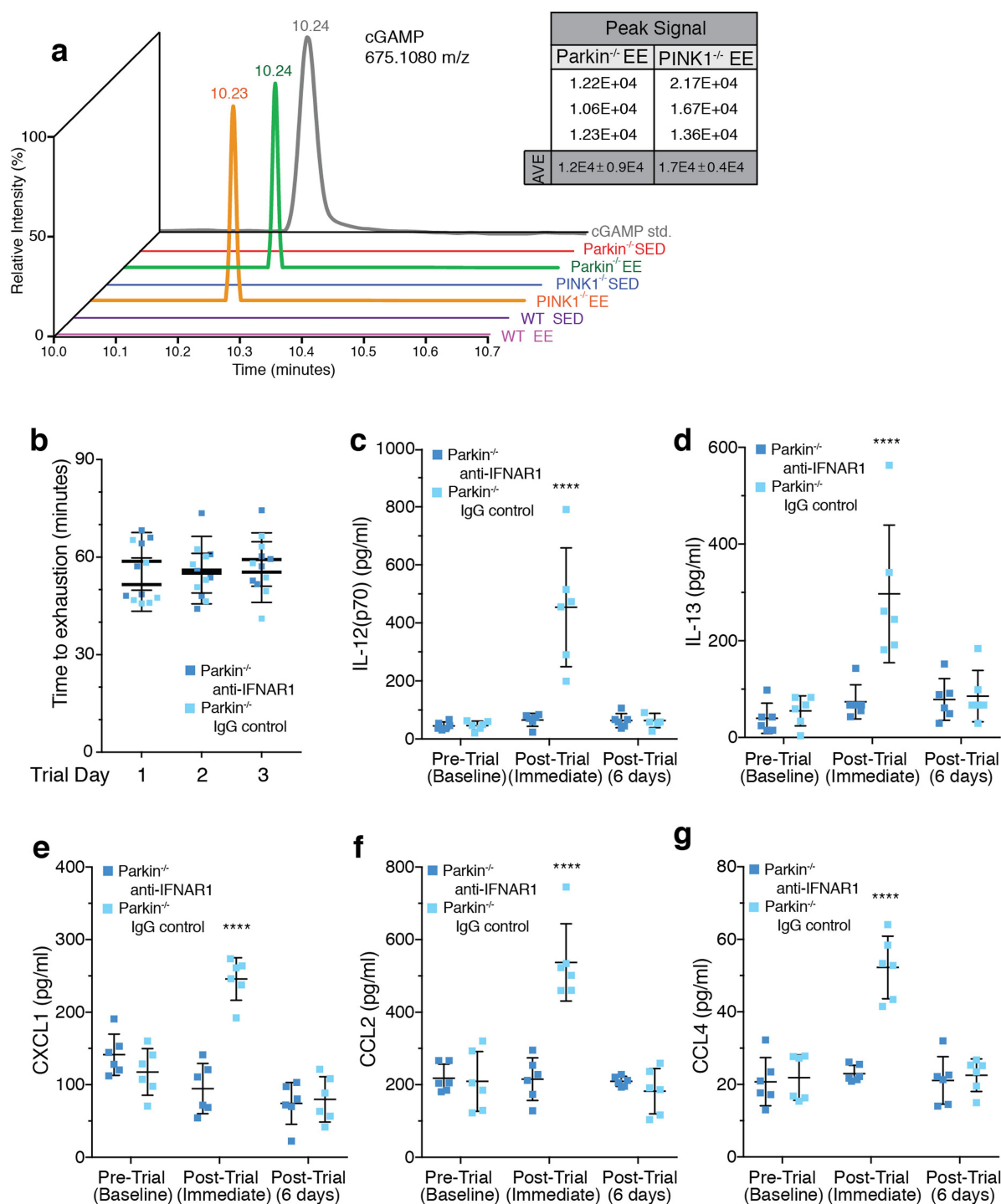
Extended Data Fig. 2 | Inflammatory cytokines are increased in mice and humans with heterozygous loss of parkin or PINK1. a–f, Serum cytokine concentrations from *Prkn*^{+/-} ($n = 4$) and *Pink1*^{+/-} ($n = 6$) EE mice. g–i, Serum cytokine concentrations from human control

(HC) ($n = 62$), *PINK1* heterozygotes (P1H) ($n = 6$), unaffected *PRKN* heterozygotes (UPH) ($n = 7$), affected *PRKN* biallelic mutants (APB) ($n = 7$) and patients with idiopathic Parkinson's disease (IPD) ($n = 9$). Data are mean \pm s.d.



Extended Data Fig. 3 | Loss of STING prevents increased cytokine levels in *Prkn*^{-/-} and *Pink1*^{-/-} mice following EE. **a**, Average time to exhaustion on each trial day (*n* = 6). **b**, **c**, Heat map depicting the average baseline serum cytokine concentration for EE mice (*n* = 6) and the

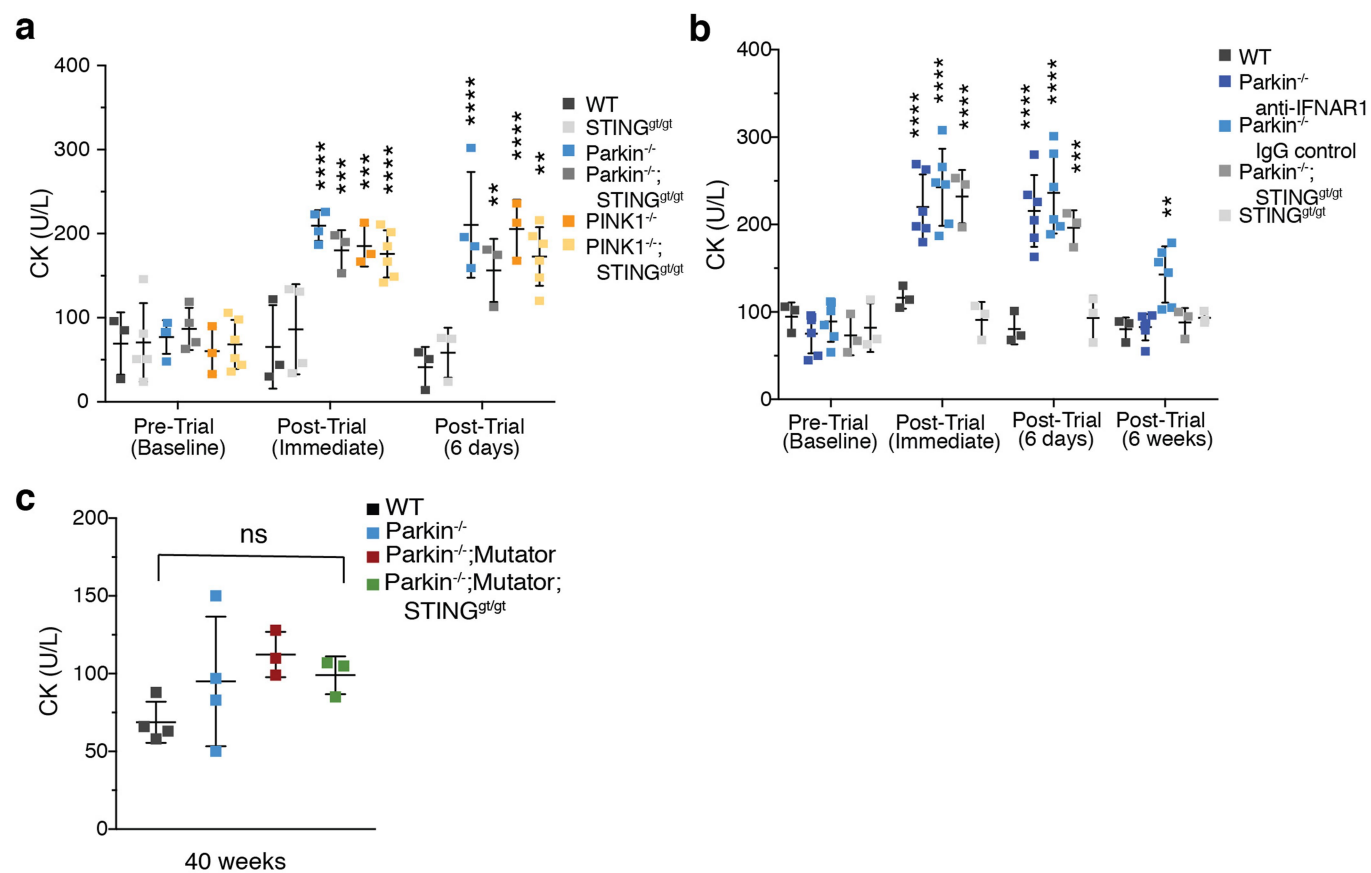
average serum cytokines from SED mice (*n* = 6). **d**–**i**, Serum cytokine concentrations from mice are plotted as mean ± s.d. (*n* = 6 baseline, post-trial immediate; *n* = 3, post-trial 2 days, post-trial 6 days).



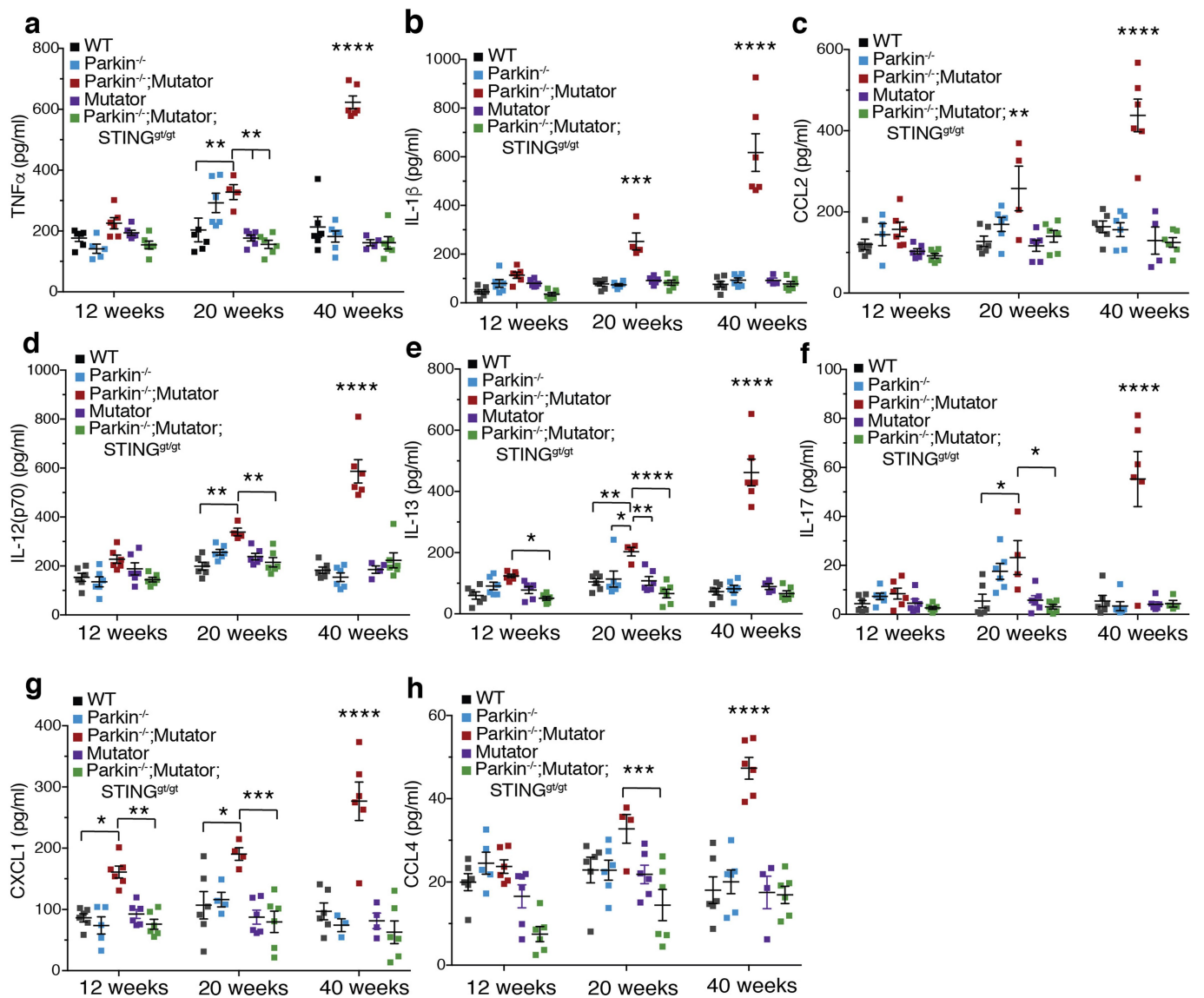
Extended Data Fig. 4 | cGAMP is increased in *Prkn*^{-/-} and *Pink1*^{-/-} EE heart tissue and inflammation is inhibited by anti-IFNAR1 treatment.

a, Representative plot of signal intensity for cGAMP measured in heart tissue. cGAMP was not detected in wild-type EE or in SED mice. Average

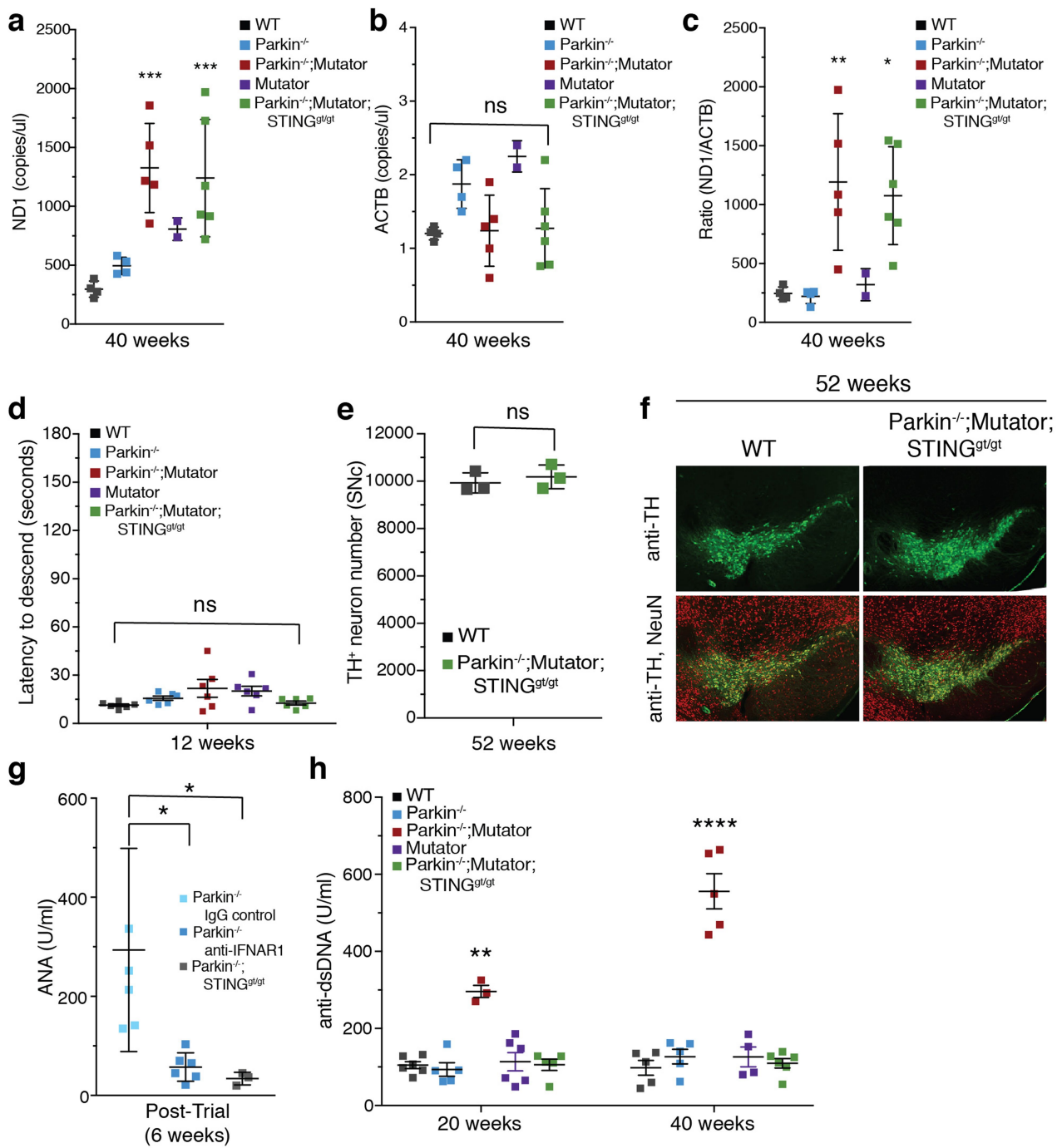
signal intensity for $n=3$ samples is shown in the inset. **b**, Average time to exhaustion on each trial day ($n=6$). **c–g**, Serum cytokine concentrations from EE *Prkn*^{-/-} mice treated with anti-IFNAR1 antibody or IgG control ($n=6$). Data are mean \pm s.d.



Extended Data Fig. 5 | Elevated serum creatine kinase following EE in *Prkn*^{-/-} and *Pink1*^{-/-} mice is not rescued by inhibition of inflammation and is not increased by chronic mitochondrial dysfunction. a–c, Serum creatine kinase (CK) levels ($n < 3$). Data are mean \pm s.d.



Extended Data Fig. 6 | Inflammation in aged *Prkn* $^{-/-}$; *mutator* mice is rescued by loss of STING. a–h, Serum cytokine concentrations from 12, 20 and 40-week-old mice ($n = 4, 6$). Data are mean \pm s.d.



Extended Data Fig. 7 | STING mediates inflammation under chronic mitochondrial stress. **a, b**, Copy number per μl of cell-free mtDNA (ND1) or nuclear DNA (ACTB) in serum ($n < 3$). **c**, Ratio of mtDNA to nuclear DNA. ($n < 3$). **d**, The time required for 12-week-old mice to descend the pole ($n = 6$). **e**, TH⁺-neurons counted by stereology in the substantia nigra (SNC) of 52-week-old mice ($n = 3$). **f**, Representative images of

TH⁺ neurons (green) and total neurons (NeuN, red). **g**, Serum levels of antinuclear antibodies (ANA) 6 weeks post-EE. dsDNA antibodies were not detected and ANAs were not detected at baseline or immediately post-EE ($n = 4, 6$). **h**, Serum levels of anti-dsDNA antibodies ($n = 4, 6$). ANA antibodies were not detected. Data are mean \pm s.d. ($n = 6$).

Life Sciences Reporting Summary

Nature Research wishes to improve the reproducibility of the work that we publish. This form is intended for publication with all accepted life science papers and provides structure for consistency and transparency in reporting. Every life science submission will use this form; some list items might not apply to an individual manuscript, but all fields must be completed for clarity.

For further information on the points included in this form, see [Reporting Life Sciences Research](#). For further information on Nature Research policies, including our [data availability policy](#), see [Authors & Referees](#) and the [Editorial Policy Checklist](#).

Please do not complete any field with "not applicable" or n/a. Refer to the help text for what text to use if an item is not relevant to your study. For final submission: please carefully check your responses for accuracy; you will not be able to make changes later.

▶ Experimental design

1. Sample size

Describe how sample size was determined.

No methods were used to determine sample size. Our first analysis used 10 mice (Figure 1) and the differences were so dramatic and consistent that in the spirit of the 3 R's of animal research we reduced the number to 4 or 6 for remaining experiments.

2. Data exclusions

Describe any data exclusions.

Two mice were removed from the study. One because it never exercised well on the treadmill, not running for more than 30 minutes, and the second was found to have a leg deformity upon euthanasia. We felt that failing to run or a bone defect could skew data.

3. Replication

Describe the measures taken to verify the reproducibility of the experimental findings.

Each experiment used a new cohort of mice with very consistent results. Methods sections are as precise as possible. Mice in Figures 4 and ED 6,7 were subjected to repeated trials at 12, 20 and 40 weeks. .

4. Randomization

Describe how samples/organisms/participants were allocated into experimental groups.

Mice were assigned randomly to each experimental groups (sedentary or exhaustive exercise) with matched male and female numbers.

5. Blinding

Describe whether the investigators were blinded to group allocation during data collection and/or analysis.

The experimenters were blinded to drug treatments and for all serum analysis. Body Temp and run times were measured in a blinded manner for experiments in Figure 2.

Note: all in vivo studies must report how sample size was determined and whether blinding and randomization were used.

6. Statistical parameters

For all figures and tables that use statistical methods, confirm that the following items are present in relevant figure legends (or in the Methods section if additional space is needed).

n/a Confirmed

- The exact sample size (n) for each experimental group/condition, given as a discrete number and unit of measurement (animals, litters, cultures, etc.)
- A description of how samples were collected, noting whether measurements were taken from distinct samples or whether the same sample was measured repeatedly
- A statement indicating how many times each experiment was replicated
- The statistical test(s) used and whether they are one- or two-sided
Only common tests should be described solely by name; describe more complex techniques in the Methods section.
- A description of any assumptions or corrections, such as an adjustment for multiple comparisons
- Test values indicating whether an effect is present
Provide confidence intervals or give results of significance tests (e.g. P values) as exact values whenever appropriate and with effect sizes noted.
- A clear description of statistics including central tendency (e.g. median, mean) and variation (e.g. standard deviation, interquartile range)
- Clearly defined error bars in all relevant figure captions (with explicit mention of central tendency and variation)

See the web collection on [statistics for biologists](#) for further resources and guidance.

► Software

Policy information about [availability of computer code](#)

7. Software

Describe the software used to analyze the data in this study.

2-WAY ANOVA statistical tests for multiple comparisons, or when appropriate Student T-tests were performed with PRISM 7 as noted in methods or figure legends

For manuscripts utilizing custom algorithms or software that are central to the paper but not yet described in the published literature, software must be made available to editors and reviewers upon request. We strongly encourage code deposition in a community repository (e.g. GitHub). *Nature Methods* [guidance for providing algorithms and software for publication](#) provides further information on this topic.

► Materials and reagents

Policy information about [availability of materials](#)

8. Materials availability

Indicate whether there are restrictions on availability of unique materials or if these materials are only available for distribution by a third party.

There are no restrictions

9. Antibodies

Describe the antibodies used and how they were validated for use in the system under study (i.e. assay and species).

the anti-IFNAR1 mouse antibody and the human IgG control used in vivo are listed clearly with referencing manuscript in the methods.

10. Eukaryotic cell lines

a. State the source of each eukaryotic cell line used.

no cell lines were used

b. Describe the method of cell line authentication used.

n/a

c. Report whether the cell lines were tested for mycoplasma contamination.

n/a

d. If any of the cell lines used are listed in the database of commonly misidentified cell lines maintained by [ICLAC](#), provide a scientific rationale for their use.

n/a

► Animals and human research participants

Policy information about [studies involving animals](#); when reporting animal research, follow the [ARRIVE guidelines](#)

11. Description of research animals

Provide all relevant details on animals and/or animal-derived materials used in the study.

The mouse strains used (strain number and source), as well as their husbandry care, are clearly listed in the methods section.

Policy information about [studies involving human research participants](#)

12. Description of human research participants

Describe the covariate-relevant population characteristics of the human research participants.

We have included a supplemental excel file that lists all relevant data as well as a reference for a paper describing the cohort. If more information is found to be needed we are happy to supply.